Title

Untangling impacts of global warming and Interdecadal Pacific Oscillation on long-term variability of North Pacific tropical cyclone track density

Journal

Science Advances, 6(41)

ISSN

2375-2548

Authors

Zhao, Jiuwei
Zhan, Ruifen
Wang, Yuqing
et al.

Publication Date

2020-10-09

DOI

10.1126/sciadv.aba6813

Peer reviewed

CLIMATOLOGY

Untangling impacts of global warming and Interdecadal Pacific Oscillation on long-term variability of North Pacific tropical cyclone track density

Jiuwei Zhao[1,2,3,4]*, Ruifen Zhan[1]*, Yuqing Wang[2†], Shang-Ping Xie[5], Qiong Wu[3,4]

How much the observed long-term variability of tropical cyclone (TC) activity is due to anthropogenic global warming (GW) or internal climate variability remains unclear, limiting the confidence in projected future change in TC activity. Here, the relative contributions of GW and the Interdecadal Pacific Oscillation (IPO) to the long-term variability of TC track density (TCTD) over the North Pacific (NP) are quantified on the basis of statistical analyses and climate model simulations. Results show that historical GW mainly reduced (increased) TCTD over the western (eastern) NP, while the positive (negative) IPO corresponds to a NP basin–wide increase (decrease) in TCTD except in some coastal regions. The IPO has a much greater impact on TCTD over the western NP than GW, while the IPO and GW impacts are about equal over the eastern NP during 1960–2019. These findings have important implications for projecting future TC activity over the NP.

INTRODUCTION

Tropical cyclones (TCs) are among the most devastating weather systems and can cause large casualties and heavy property losses. The western North Pacific (WNP) features the largest number of TCs, while the eastern NP (ENP) has the most TCs per unit area of any basin worldwide (*1*). Given that TC tracks affect TC landfall location, it is of great importance to elucidate the underlying causes of the observed long-term variability in TC tracks over the NP. Anthropogenic global warming (GW) has been recognized to affect the observed long-term trends in TC tracks (*2*), but the effect remains uncertain because it is difficult to estimate whether the anthropogenic effect exceeds the level expected from interdecadal climate variability because of the limited length of data records (*3*, *4*). Some studies suggested that the observed trends in TC track density (TCTD; storms in unit grid box) over the WNP are likely due to internal climate variability (*5*, *6*), such as the Interdecadal Pacific Oscillation (IPO) (*7*, *8*). The IPO is the dominant mode of interdecadal variability over the Pacific with the sea surface temperature (SST) pattern similar to that of the El Niño–Southern oscillation (*9*). For the ENP, although no significant trends in total number of TCs have been found (*7*, *9*, *10*), interdecadal variability in both TC tracks and landfalling TCs is evident on the Pacific coast of Mexico because of the IPO modulations (*9*, *11*).

The majority of climate models projected an eastward shift of TCTD from the WNP to the central NP (*12*, *13*), with decreased TCTD over the WNP (*14*, *15*) and increased TCTD over the ENP (*16*, *17*) in warming climate, while a few models suggested a pronounced increase over the WNP (*18*) and decrease over the ENP (*19*). These uncertainties could be introduced by the stark difference in zonal SST pattern among the models (*20*–*23*) or could be related to a tangled interaction between GW and internal climate variability (*22*, *24*, *25*). Although the statistical relationship of TCTD with either SST warming trend or the IPO has been previously studied, the relative contributions of GW and the IPO to the long-term changes in TCTD remain to be quantified and the dynamical mechanisms remain to be poorly understood (*6*, *26*). Here, we use the ensemble empirical mode decomposition (EEMD) method (*27*) to derive the GW and the IPO modes and examine their impacts on TCTD based on the historical TC best-track data and several commonly used global reanalysis datasets. This is followed by a suite of climate model experiments. We quantify the relative contributions of GW and the IPO to the long-term variability of TCTD over the NP based on a linear regression model and high-resolution atmospheric general circulation model (HIRAM). Results show that the IPO contributes more to the long-term variability of TCTD than GW over the WNP, while they contribute about equally to that over the ENP. These findings help resolve the ongoing debate as to whether the long-term variability in TCTD is primarily due to GW or internal climate variability, with important implications for projections of future TC activity over the NP.

Effects of GW and the IPO on TCTD over the NP

The EEMD method (*27*) has been widely used to derive atmospheric or oceanic modes even if they are nonstationary and nonlinear (*28*–*30*). Usually, the last (here, the 10th) intrinsic mode function (IMF) of EEMD can present the GW trend, while the combination of the sixth to ninth IMF represents the interdecadal variability based on the monthly raw SST data [(*29*); an example is shown in fig. S1]. A statistically significant GW trend in SST over 45°S to 45°N and 0° to 360° for the period 1960–2019, with significance above 95% confidence levels based on the Mann-Kendall trend test, was derived from the 10th EEMD IMF (Fig. 1A), which is defined as the GW index in this study. The spatial SST increments exhibit an overall GW pattern with the most pronounced warming in the tropical Indian Ocean, the warm pool region over the WNP, and the tropical Atlantic (Fig. 1B). However, the warming rate is lower over the central

[1]Department of Atmospheric and Oceanic Sciences and Institute of Atmospheric Sciences, Fudan University, Shanghai, China. [2]International Pacific Research Center and Department of Atmospheric Sciences, School of Ocean and Earth Science and Technology, University of Hawaii at Manoa, Honolulu, HI, USA. [3]Division of Environmental Science and Engineering, Pohang University of Science and Technology (POSTECH), Pohang, South Korea. [4]Key Laboratory of Meteorological Disaster of Ministry of Education (KLME), Nanjing University of Information Science and Technology, Nanjing, China. [5]Scripps Institution of Oceanography, University of California San Diego, La Jolla, CA, USA.
*These authors contributed equally to this work.
†Corresponding author. Email: yuqing@hawaii.edu

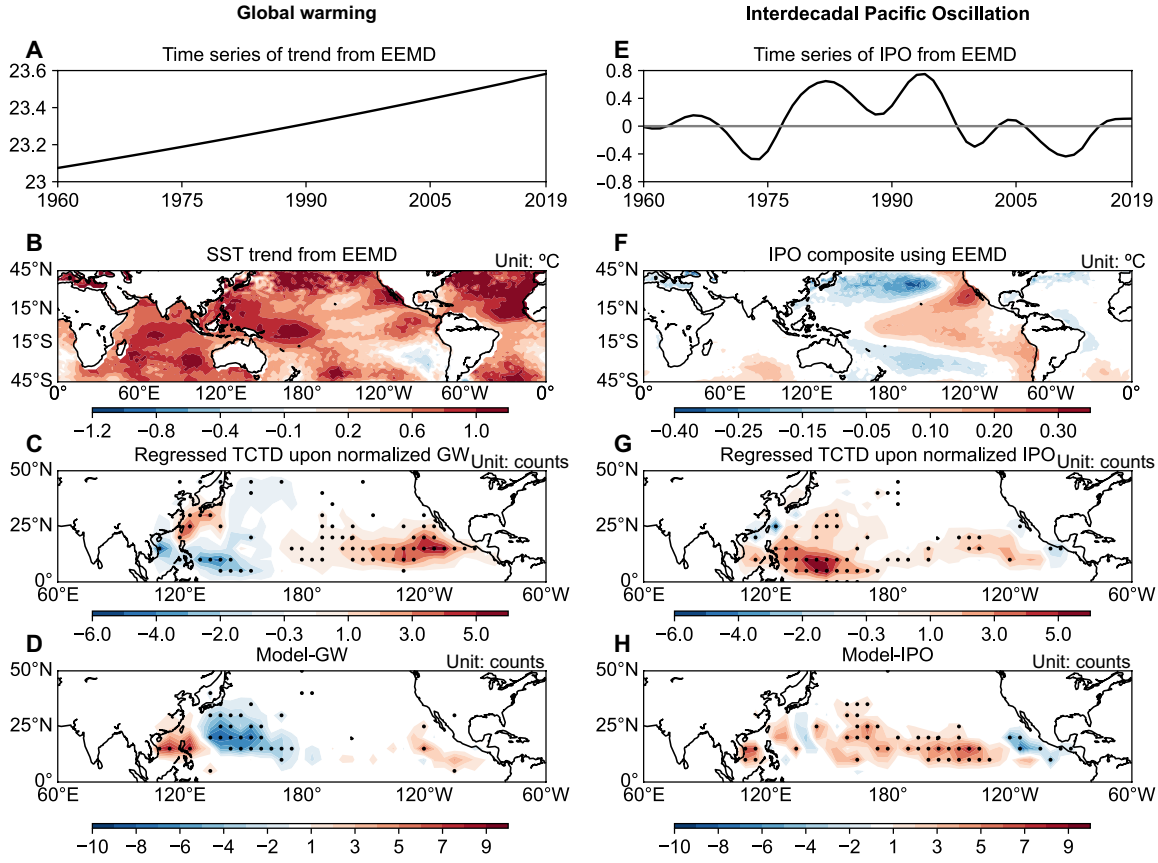

Fig. 1. GW and IPO modes, and their effects on TCTD over the NP. The left panel shows the GW analysis, and the right panel is the analysis based on the IPO phases. (**A**) The GW time series derived from the 10th IMF of EEMD of monthly SST (°C) averaged over the globe (45°S to 45°N and 0° to 360°) for the period 1960–2019. (**B**) The trend increments in each grid point of the 10th IMF of global SST (°C). (**C**) Regressed SST (°C) and (C) TCTD upon the normalized GW time series in (A). (**D**) The TCTD difference between the GW and CTRL runs. (**E**) The IPO time series derived from the combination of the sixth to ninth IMF of EEMD of the monthly raw IPO index for the period 1960–2019. (**F**) Composite of SST between positive and negative IPO phases. (**G**) Regressed TCTD upon the normalized IPO time series in (E). (**H**) Same as (D) but between the IPO and CTRL runs. The black dots in (C), (D), (G), and (H) show areas where the statistical significance is above 90% confidence level based on two-tailed Student's *t* test.

Pacific than over other tropical oceans, showing a "La Niña–like" SST pattern, consistent with recent findings (*21*, *31*–*33*). The regressed June to November averaged TCTD upon the normalized GW index during 1960–2019 shows decreasing trends over most of the WNP except for the coastal regions off East China but increasing trends over the central NP and the ENP (Fig. 1C), indicating a robust decrease in TCTD averaged over the whole WNP and an increase over the ENP. Although this is consistent with most previous projections (*16*, *18*), the La Niña–like SST pattern here is distinct from the El Niño–like SST pattern projected by most climate models (*34*). Results based on observational data analyses above are confirmed by a suite of numerical experiments (see Materials and Methods). The GW run generally reproduced the observed responses of TCTD to GW (Fig. 1D). The TCTD simulated in the GW run shows a significant decrease over the WNP and an increase over the ENP, despite some discrepancies such as an increase in the South China Sea and a decrease along Japan and Korea.

The time series derived from the combination of the sixth to ninth IMF of EEMD based on the raw monthly IPO index (*35*) shows a clear interdecadal variability, in positive phase during 1977–1997 and negative phase before 1977 and during 1997–2014 (Fig. 1E). The composite SST between positive and negative IPO phases obtained from the sixth to ninth IMF is characterized by the tripole-SST pattern with positive SST anomalies (SSTAs) over the tropical Pacific and negative SSTAs over the subtropics in both hemispheres (Fig. 1F). During the positive IPO phase, the regressed positive anomalies of June to November averaged TCTD cover the whole NP except for the coastal regions off East Asia in the WNP and central America in the ENP (Fig. 1G), consistent with previous studies (*8*, *11*). The TCTD simulated in the IPO run (Fig. 1H) exhibits an overall increase over the NP except for a large decrease in the coastal regions of the ENP and East Asia. The GW and IPO simulations generally confirm the overall features obtained from observational data analyses above, suggesting that our statistical methods can reasonably isolate the individual contributions of GW and the IPO to the long-term variability in TCTD over the NP.

To confirm the close relationship between the above two SST modes and TCTD over the NP, we also examine the coupled modes between June to November averaged SSTs (between 45°S and 45°N) and TCTD (unit: storms/5° × 5°) over the NP for the period 1960–2019 based on the singular value decomposition (SVD) analysis (fig. S2). The first two SVD modes of SST (accounting for 43.2% and

20.2% of the total covariance) show a La Niña–like warming pattern and a significant positive IPO pattern, respectively, consistent with the results from EEMD (Fig. 1, B and E). The first SVD mode of TCTD, which reflects the response to GW, shows a robust decrease over the WNP and an increase over the ENP. The second SVD mode, which is related to the positive IPO phase, shows positive anomalies over the whole NP except for the coastal regions off East Asia and the ENP. These are consistent with the results from the linear regressions (Fig. 1, C and F). The linear trends in both SST and TCTD and their interdecadal composites between positive and negative IPO phases (fig. S3) are generally in good agreement with those based on EEMD (Fig. 1) and SVD analyses (fig. S2). These results demonstrate that both La Niña–like GW and the IPO contributed to the long-term variability of TCTD over the NP. Note that the long-term variability beyond the interannual time scale accounts for 51.5% of the total variance of TCTD over the WNP and 38.4% over the ENP.

Mechanisms for long-term variability in TCTD over the NP

To understand the mechanisms by which GW and the IPO affect TCTD over the NP, we examine the variations of the large-scale environments that control TCTD, including the low-level winds (LLW), 850-hPa relative vorticity (Vor), vertical zonal wind shear (VZWS) between 200 and 850 hPa, and steering flow (SF). TCTD depends primarily on its genesis location and subsequent movements. In general, at low levels, westerly anomalies over the tropics with anomalous cyclonic shear Vor off the equator, an anomalous cyclonic circulation in the lower troposphere, and a weak VZWS are favorable for TC genesis and development, while the large-scale SF is essential for TC movement.

Figure 2 shows the long-term trends and the composite differences between the positive and negative IPO phases for June to November averaged LLW and Vor, VZWS, and SF based on the National Oceanic and Atmospheric Administration (NOAA) 20 Century (20C) reanalysis. In response to GW, the LLW shows a significant divergent trend over the central Pacific (Fig. 2A), with low-level easterly winds increasing over the tropical WNP and decreasing over the tropical ENP and a small anomalous cyclone over the coastal region off East Asia. Similarly, the Vor field shows significant negative anomalies over most of the WNP and positive anomalies over the ENP, with small positive anomalies over the

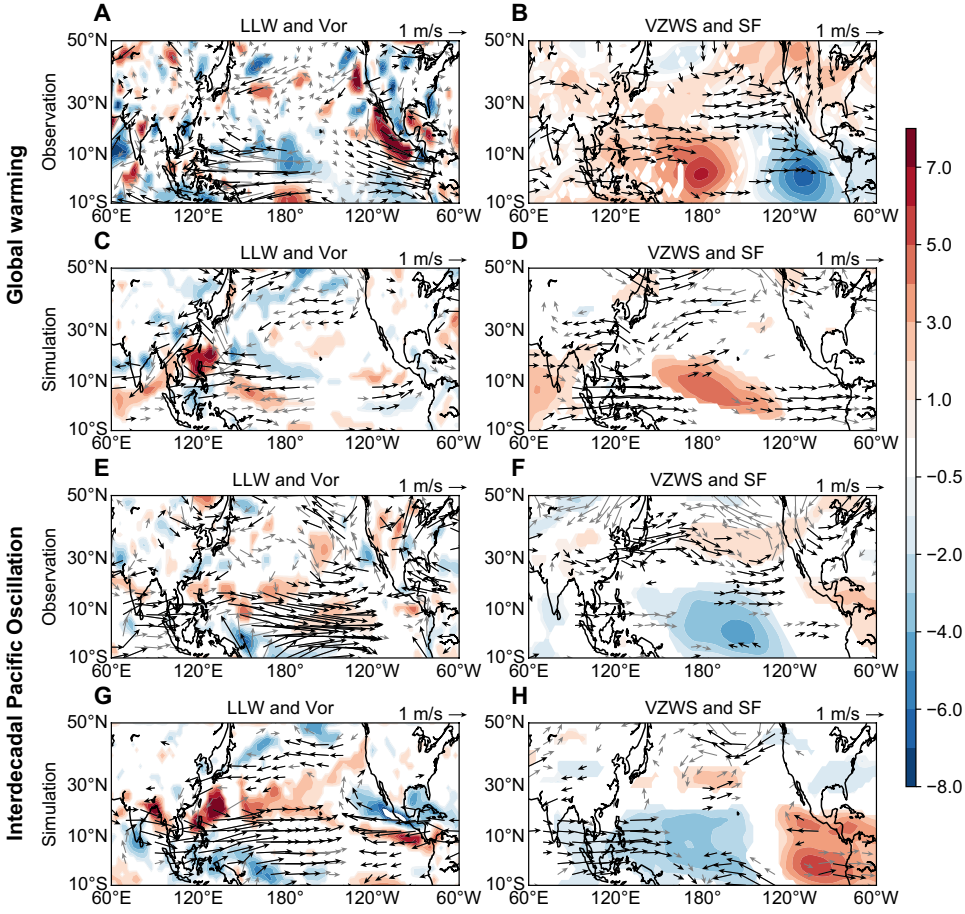

Fig. 2. Modulation of GW and the IPO to the large-scale environments that control TCTD. Trends (**A** to **D**) and composites (**E** to **H**) of (left) 850-hPa LLW (m s^{-1}; vector) and 850-hPa relative Vor (5×10^{-7} s^{-1}; shaded) and (right) SF (m s^{-1}; vector) and VZWS (m s^{-1}; shaded) between 200 and 850 hPa from (A, B, E, and F) observations and (C, D, G, and H) model simulations. The top two rows represent the circulation anomalies affected by GW from both observation and simulation, and the lower two rows indicate that influenced by the IPO. In observation, the long-term trends were calculated during 1960–2014 and the composite differences were calculated between the positive (1977–1997) and negative (1960–1976 and 1998–2014) IPO phases. In the simulations, the differences between the GW and CTRL runs (C and D) and between the IPO and CTRL runs (G and H) were conducted. The shaded and black vectors in (A) and (B) represent areas that are statistically significant above 90% confidence level based on two-sided Mann-Kendall trend test, while those in (C) to (H) show areas where the statistical significance is above 90% confidence level based on two-tailed Student's *t* test.

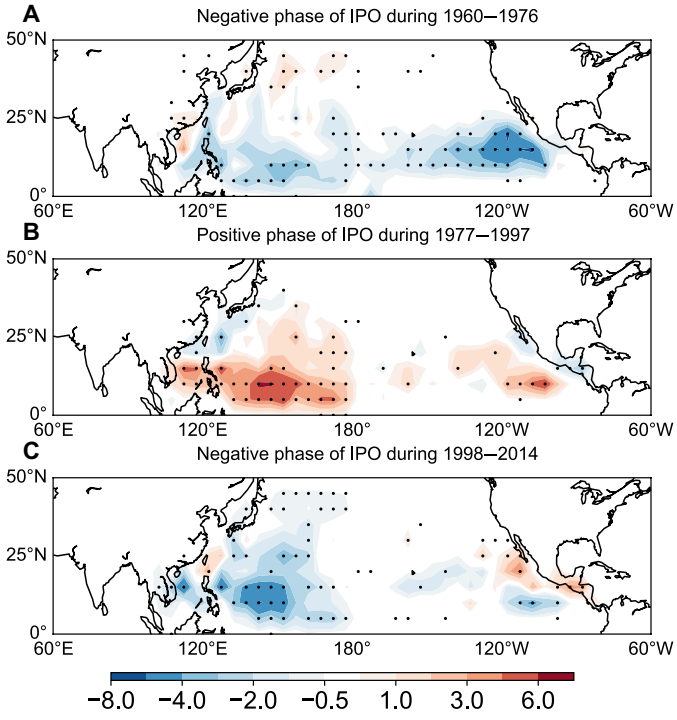

Fig. 3. TCTD (unit: counts) anomalies in different IPO phases relative to the climatological TCTD (unit: counts), which is defined as the average during 1960–2019. The TCTD anomalies in the negative IPO phase during 1960–1976 (**A**), in the positive IPO phase during 1977–1997 (**B**), and in the recent negative IPO phase during 1998–2014 (**C**). The black dots represent areas where the statistical significance is above 90% confidence level based on two-tailed Student's *t* test.

coastal region off East Asia, where relatively faster warming occurred (Fig. 1B) with large maximum potential intensity (MPI) trends (fig. S6C). The VZWS exhibits an increasing trend over the WNP centered on the equator and decreasing trend over the ENP (Fig. 2B). Previous studies have shown that the VZWS over the equatorial Pacific plays a crucial role in affecting TC activity over the WNP (*36*, *37*). These trends in LLW and VZWS generally suppress local TC genesis and reduce TCTD over the WNP but promote TC genesis/intensification and increase TCTD in the coastal regions off East Asia and the ENP. Over the WNP, changes in large-scale SF (Fig. 2B) are westerly south of 25°N, reducing TCTD over South China. Over the ENP, the anomalous westerly SF strengthened TC activity along the coastal area of the ENP. In addition, the increasing trends in 600-hPa relative humidity are also favorable for TC genesis over the ENP while unfavorable over the WNP (fig. S4). These are consistent with the effect of the La Niña–like SST warming (namely, GW) on TCTD in the NP (Fig. 1, B and C).

Figure 2 (E and F) shows the composite differences in LLW, Vor, VZWS, and SF between the positive (1977–1997) and negative (averaged on the two periods of 1960–1976 and 1998–2014) IPO phases. In the positive phase, the tropical Pacific is dominated by anomalous low-level westerlies associated with positive Vor anomalies and weakening VZWS over the tropical western and eastern Pacific. These large-scale anomalies are favorable for TC genesis and intensification over both the WNP and ENP. Note that the favorable environmental conditions in the positive IPO phase are mainly located over the open ocean far away from the coasts where more TCs formed on the basis of the SVD analysis (fig. S5). Once TCs form over the open ocean, they are likely to last longer compared with those near coastal regions, thereby increasing TCTD. However, the composite differences in large-scale SF show an overall intensifying offshore flow south of 25°N over the WNP and weakening SF along the coast of the ENP, suggesting that the positive IPO generally enhances TCTD over the open ocean and suppresses TC activity over the coastal regions of the NP.

Table 1. The annual mean TC genesis frequency and TCTD in June to November from the best-track TC data and three numerical experiments over the WNP and ENP for the period 1990–2009. The TCTD is calculated over 100°E to 180°, EQ to 40°N. The boldface values are statistically significant at 90% confidence levels based on two-sided Student's *t* test when comparing the time series of a sensitivity run and a CTRL run. The values with underscore are statistically significant at 90% confidence levels based on chi-square test. TCGF, TC genesis frequency.

	WNP		ENP	
	TCGF	TCTD	TCGF	TCTD
Observations	22.5	843	15.7	416
CTRL	24.9	751	16.3	337
GW	22.8	**650**	**19.5**	**379**
IPO	**28.9**	**913**	**20.4**	**391**

We have examined the linear trend and IPO composites of genesis potential index (GPI) and MPI (fig. S6). The trend in GPI over the WNP and the ENP is generally consistent with that in TCTD. However, the IPO impact on GPI is not consistent with that on TCTD over most of the WNP, suggesting that the increased TCTD there is not caused by the trend in TC genesis. The MPI could partly explain the positive trend in TCTD over the northern WNP and higher TCTDs over the ENP in the positive IPO phase. We also examined the trend and composite fields in large-scale conditions based on the National Centers for Environmental Prediction/National Centers for Atmospheric Research reanalysis, and the overall patterns of these changes (fig. S7) are highly consistent with those reported here from the 20C reanalysis.

The GW run with the model (Fig. 2, C and D) reproduces the increase in low-level easterly and VZWS over the WNP and the central Pacific with a little eastward shift. However, the model fails to reproduce the negative trend in VZWS over the ENP. The positive IPO run (Fig. 2, G and H) reproduces anomalous low-level westerly and weakened VZWS over the tropical Pacific. These results are generally consistent with those obtained on the basis of the reanalysis data discussed above, although some model biases exist in the large-scale fields over the South China Sea and along the coast of the ENP.

Relative importance of GW and the IPO

The TCTD over the WNP exhibits pronounced interdecadal variability (Fig. 3), switching from negative anomalies during 1960–1976 to positive anomalies during 1977–1997 and changing back to negative anomalies during 1998–2014. This is in good agreement with IPO phase changes, suggesting that the IPO plays a more important role in the long-term variability of TCTD over the WNP than GW. In comparison, the TCTD change over the ENP is more complicated. Although the TCTD anomalies switched from negative

during 1960–1976 to positive during 1977–1997, the negative and positive values coexisted during 1998–2014, suggesting that GW and the IPO might be equally important over the ENP because GW and the negative IPO have opposite effects on TCTD during 1998–2014 (Fig. 1, C and F).

The relative importance of GW and the IPO for the long-term variability of TCTD is quantified using a linear regression model based on the GW and IPO indices derived from EEMD (Fig. 1, A and D). Results show that the GW and IPO modes together explain 55.4% and 60.8% of the long-term variance of TCTD (fig. S8) during 1960–2019 over the WNP and the ENP, respectively. Of the 55.4% variance over the WNP, the GW contributed 35.9% (19.9% variance) and the IPO contributed 64.1% (35.5% variance), while of the 60.8% variance over the ENP, the GW and the IPO contributed 57.2% (34.8% variance) and 42.7% (26% variance), respectively. The chi-square test shows that the difference in contribution between GW and IPO over the WNP is significant at 95% confidence level, while the difference over the ENP is insignificant, suggesting that the IPO contributes much more to the long-term variability of TCTD than GW over the WNP, while GW and the IPO contribute about equally over the ENP.

We also examined the TCTD in model experiments. TCTD in the GW run is lower averaged over the WNP and higher averaged over the ENP than in the control run while increasing in the positive IPO run over both the sub-basins (Table 1). Over the WNP, the TCTD anomalies are smaller in the GW than IPO run, suggesting a greater IPO effect (Table 1). Over the ENP, the difference is insignificant, suggesting that GW and the IPO are about equally important to the long-term variability of TCTD (Table 1). These are consistent with our results based on the TC best-track data and linear regression model.

Since the TCTD is closely related to the genesis locations and the subsequent TC motions, its variability can be decomposed into three terms: genesis, track, and nonlinear terms (see Materials and Methods) (*15*, *31*); the relative contributions of GW and IPO to these three terms can be statistically estimated. Results show that the significant decreasing trend in TCTD over the WNP due to GW (Fig. 4A) is largely contributed by the TC genesis location (Fig. 4B), while the TC track and nonlinear terms contribute to both poleward

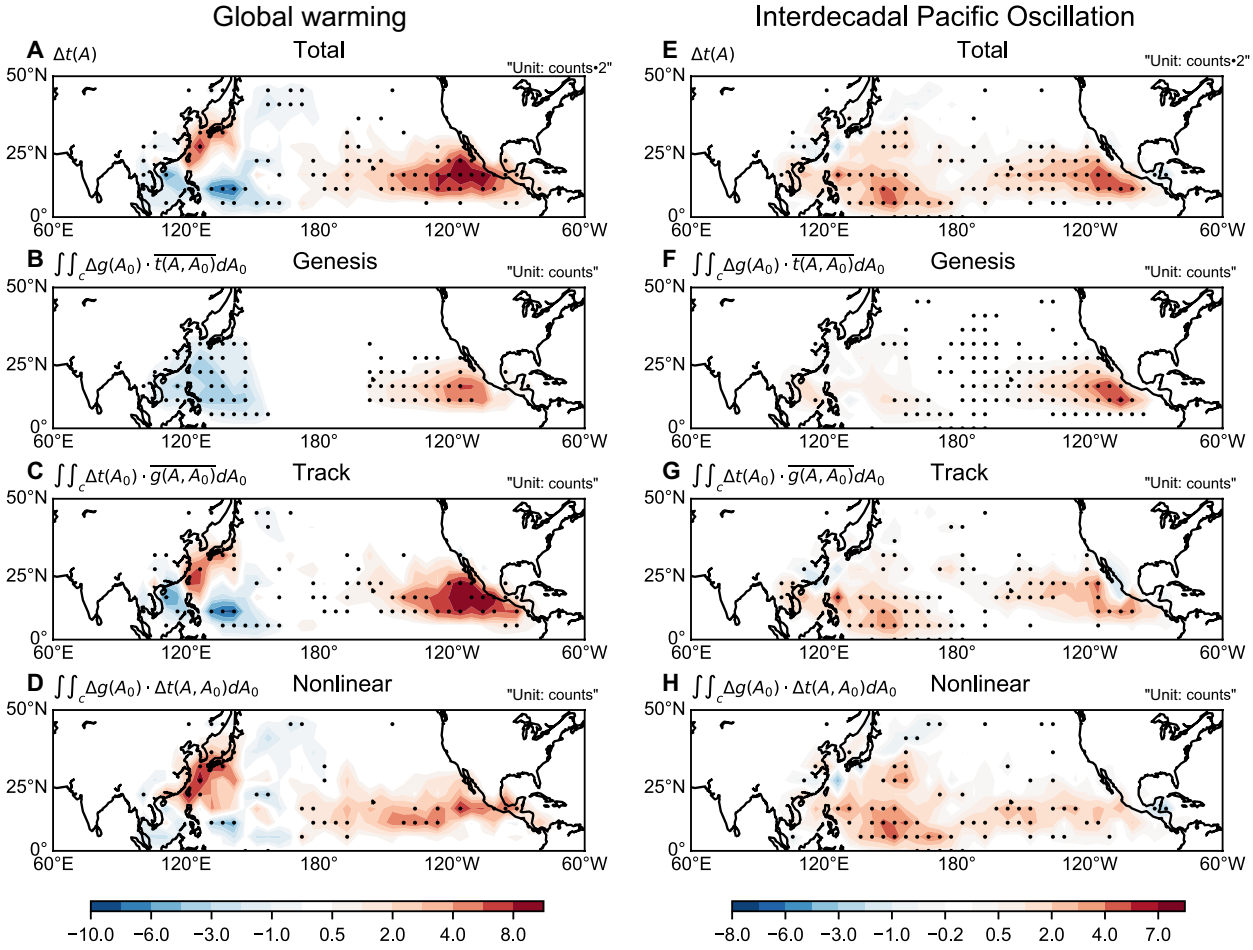

Fig. 4. Relative contributions of GW and IPO to TCTD by TC genesis, track, and nonlinear terms for the period 1960–2019. Trend increments in TCTD from 1960–2019 (**A**) and contributions by genesis location (**B**), tracks (**C**), and nonlinear effects (**D**). Composite difference in TCTD between the positive (1977–1997) and the negative (1960–1976 and 1998–2014) IPO phases (**E**) and contributions by genesis location (**F**), tracks (**G**), and nonlinear effects (**H**). The black dots in (A) to (D) represent areas where the statistical significance is above 90% confidence level based on two-sided Mann-Kendall trend test, while others in (E) to (H) show areas where the statistical significance is above 90% confidence level based on two-tailed Student's *t* test. The values in (A) and (E) are divided by a factor of 2 for sharing the same color bar. The contribution is also represented by the formulae shown in each subtitle.

and westward shifts of TCTD (Fig. 4, C and D). Over the ENP, all the three terms contribute to the increasing trend of TCTD in response to GW, with the largest contribution from the track term. Note that although the overall decreasing/increasing trend in TCTD is attributed to GW, the spatial pattern of TCTD is dominated by the anomalous atmospheric circulation induced by spatial variations in SST warming (fig. S2A). This may have implications for model projections of future TC activity. The IPO composite (Fig. 4) shows that both the track and nonlinear terms predominantly contribute to the interdecadal variability in TCTD over the WNP (Fig. 4, G and H), while the genesis location and track terms contribute to TCTD variability over the ENP (Fig. 4, F and H).

DISCUSSION

In summary, we have untangled impacts of GW and the IPO on the long-term variability in NP TCTD based on observational analyses and TC-permitting model experiments. We show here that the IPO has a much greater impact on the long-term variability in TCTD over the WNP than GW, while both GW and the IPO contribute about equally over the ENP. Our results provide an initial assessment on the relative contributions of GW and the IPO to the long-term variability in NP TCTD. It is an important benchmark to evaluate climate models in their ability to reproduce the historical TC variations, a crucial step to build creditability in model-based future projections. Note that these results are obtained on the basis of the historical record during 1960–2019, which could change as the GW signal becomes larger and accelerates in the coming decades.

The IPO is in transition from the negative to a positive phase since around 2014, while an accelerated GW rate is expected, in part, from reduced aerosol cooling as developing countries act to curtail air pollution. Our results suggest that the combined IPO-GW effects may end the inactive TC epoch over the WNP since 1998 while increasing TC activity over the ENP in the coming decades. More frequent TC geneses are evident over both the WNP and ENP since 2015 (fig. S9). Moreover, the superposition of GW and the positive phase of IPO may lead to large increases in TCTD over both the WNP and ENP (Fig. 4, A and E) by enhancing the poleward (Fig. 4, C and G) and westward shifts of the TCTD pattern (Fig. 4, D and H). Thus, our findings have important implications for projections of future TC activity over the NP.

MATERIALS AND METHODS

Definitions of GW and the IPO modes

We quantified TCTD in terms of the TC tracks in each 5° by 5° grid box. TCTD in a grid box is counted once if a named TC passed (appeared in) the box. Here, we only counted the TCTD without considering storm's translational speed that has also been reported to be highly influenced by GW (*38*). The EEMD (*26*, *28*, *29*) method is used to derive the spatial pattern and temporal variation of SST. We decomposed the monthly SST in each grid point into 10 IMFs and chose the 10th IMF (residual) as the SST trend. We further used SVD to verify the GW and IPO modes. The SVD analysis, first introduced in (*39*) and further improved in (*40*), was used to identify the coupled modes between the global SSTs and NP TCTD. The GW and the IPO time series from the EEMD were used to evaluate the relative importance of GW and the IPO to the long-term variability in TCTD.

Relative importance analysis

A linear regression model (*41*) was used to evaluate the relative importance of GW and the IPO to the long-term variability in TCTD based on the two time series of GW and IPO from EEMD. This linear model with intercept can be written as

$$\mathrm{TCT}_i = \beta_0 + \beta_1 \cdot \mathrm{PC}_{i1} + \beta_2 \cdot \mathrm{PC}_{i2} + e_i \tag{1}$$

In Eq. 1, the response of object i is modeled as a linear function of regressor values $\mathrm{PC1}_{i1}$ and $\mathrm{PC2}_{i2}$ from EEMD analysis with unknown coefficients β_0, β_1, and β_2, and e_i indicates the unexplained part. The total contribution of the GW and IPO to the long-term change in TCTD is explained by the regressors (PC1 and PC2) in the model

$$R^2 = \frac{\mathrm{Model\_SS}}{\mathrm{Total\_SS}} = \frac{\Sigma_{i=1}^{t}(\widehat{\mathrm{TCT}_i} - \overline{\widehat{\mathrm{TCT}}})^2}{\Sigma_{i=1}^{t}(\mathrm{TCT}_i - \overline{\mathrm{TCT}})^2} \tag{2}$$

where $\widehat{\mathrm{TCT}_i} = = \widehat{\beta_0} + \widehat{\beta_1} \cdot \mathrm{PC_{i1}} + \widehat{\beta_2} \cdot \mathrm{PC_{i2}}$ in Eq. 2, TCT represents the TCTD, the overbar indicates the mean value of TCTD, and the angle bracket is for the value from the linear regression model. One way of looking at relative importance is to compare the relative portion of variance

$$R^2(\{\mathrm{PC}_k\}\,|S_k(r)) = R^2(\{\mathrm{PC}_k\} \cup S_k(r)) - R^2(S_k(r)) \tag{3}$$

Here, the order of the regressors is denoted by the tuple of indices $r = (r1, r2)$ and let $S_k(r)$ denote the set of regressors that entered the model before regressor PC_k in the order r. The final averaging over ordering metric proposed by Lindeman, Merenda, and Gold (LMG) can be written as

$$\mathrm{LMG}(\mathrm{PC}_k) = \frac{1}{2}\Sigma_{j=0}^{1}\left(\Sigma_{S \subseteq \{\mathrm{PC}_1, \mathrm{PC}_2\} \setminus \{\mathrm{PC}_k\}, n(S)=j} \frac{\mathrm{seq}(\{\mathrm{PC}_k\} \mid S)}{\binom{1}{j}}\right) \tag{4}$$

Relative contribution analysis

Another approach originally proposed in (*15*) and (*42*) was adopted to evaluate the relative contribution of TC genesis location and tracks in terms of local TCTD changes. The climatological mean TCTD in a specific 5° by 5° grid box can be written as follows

$$\overline{T(A)} = \iint_c \overline{g(A_0)} \cdot \overline{t(A, A_0)}\, \mathrm{dA}_0 \tag{5}$$

Here, $\overline{T}(A)$ is the TCTD in grid box A, $g(A_0)$ is the TC genesis frequency (TCGF) in grid box A_0, and $t(A, A_0)$ stands for the probability for a TC formed in grid box A_0 to travel into grid box A. The subscript C is the entire domain of the NP over which the integration is performed. For the period 1960–2019, the TCTD anomalies (Δ) relative to the climatological mean in grid box A are calculated as

$$\Delta T(A) = \iint_c \Delta g(A_0) \cdot \overline{t(A, A_0)}\, \mathrm{dA}_0 + \iint_c \Delta t(A_0) \cdot \overline{g(A, A_0)}\, \mathrm{dA}_0 + \iint_c \Delta g(A_0) \cdot \Delta t(A, A_0)\, \mathrm{dA}_0 \tag{6}$$

where the first term on the right-hand side (rhs) of Eq. 6 represents the contribution by changes in TC genesis locations to TCTD under the climatological mean TC tracks. The second term on the rhs

represents the contribution by changes in TC tracks under the climatological mean TC genesis locations. The last term represents the nonlinear contribution under the circumstance, with changes in both the TC genesis locations and tracks.

Model description, experimental design, and TC detection algorithm

The HIRAM (www.gfdl.noaa.gov/hiram-quickstart/), which has been demonstrated to have high skills in simulating TC variability including climate trends, interannual and interdecadal variabilities, and seasonal prediction in main TC basins and has been widely used in TC projections (*43*–*45*), developed at the Geophysical Fluid Dynamics Laboratory was used in this study. The dynamical core of HIRAM is discretized by the finite-volume method on a cubed-sphere grid topology with the horizontal resolution of roughly 50 km (varying from 43.5 to 61.6 km) and 32 vertical levels [details can be found in (*46*, *47*)], which can be used to explicitly extract TC-like vortex. We conducted one control and two sensitivity numerical experiments using HIRAM. The control (CTRL) run was forced by the observed monthly SST from 1990 to 2009. The GW run was identical to the CTRL run except that the linear trend increments of SSTs from 1960 to 2014 between 45°S to 45°N and 0° to 360° were added to the monthly SSTs used in the CTRL run. The IPO run was identical to the CTRL run except that the SSTAs (45°S to 45°N and 0° to 360°) between the positive and negative IPO phases were added to the monthly SSTs used in the CTRL run.

The model was integrated year by year for the period 1990–2009 with 6-hourly output of sea level pressure, 850-hPa Vor, temperature anomaly averaged between 500 and 300 hPa representing the TC warm core, and the 10-m winds. A well-known TC detection algorithm (www.gfdl.noaa.gov/tstorms/) was used to detect TCs in the simulations.

Our analyses only focused on the domain south of 40°N over the NP because the model has large bias in simulating TC tracks north of 40°N (fig. S10). The simulated TCGF and TCTD over the WNP and ENP in the CTRL run are generally close to those obtained from the best-track data. We also notice that the model underestimates the observed TCTD by about 11% over the WNP and 19% over the ENP (Table 1), respectively, which might be due to shorter tracks in the model simulation. Because we focused on the relative changes among the three experiments, the above model bias does not affect our overall conclusions.

Statistics

The statistical significance was checked on the basis of four methods: the two-sided Mann-Kendall trend tests, the two-tailed Student's *t* tests, the two-sided bootstrap resampling, and the chi-square test. The Mann-Kendall trend test was adopted in testing if trends of SST, TCTD, or atmospheric fields are statistically significant. The Student's *t* test was used in testing whether the two samples (composites) are significantly different from each other. The degree of freedom of the Student's *t* test is 53 for the composites of TC tracks and 20C reanalysis and 38 for the differences in model experiments. The bootstrap test was used to evaluate the robustness of relative importance analysis. For the above three test methods, it was treated as significance at 90% confidence level if the difference was above 5th or 95th percentiles. The chi-square test is used to check the significance of contribution between GW and IPO over each basin with the degree of freedom 1.

SUPPLEMENTARY MATERIALS

Supplementary material for this article is available at http://advances.sciencemag.org/cgi/content/full/6/41/eaba6813/DC1

REFERENCES AND NOTES

1. F.-F. Jin, J. Boucharel, I.-I. Lin, Eastern Pacific tropical cyclones intensified by El Niño delivery of subsurface ocean heat. *Nature* **516**, 82–85 (2014).
2. W. Mei, S.-P. Xie, Intensification of landfalling typhoons over the northwest Pacific since the late 1970s. *Nat. Geosci.* **9**, 753–757 (2016).
3. J. C. L. Chan, Comment on "Changes in tropical cyclone number, duration, and intensity in a warming environment". *Science* **311**, 1713 (2006).
4. M. J. Burn, S. E. Palmer, Atlantic hurricane activity during the last millennium. *Sci. Rep.* **5**, 12838 (2015).
5. C.-H. Ho, J.-J. Baik, J.-H. Kim, D.-Y. Gong, C.-H. Sui, Interdecadal changes in summertime typhoon tracks. *J. Climate* **17**, 1767–1776 (2004).
6. K. S. Liu, J. C. L. Chan, Interdecadal variability of Western North Pacific tropical cyclone tracks. *J. Climate* **21**, 4464–4476 (2008).
7. P. J. Webster, G. J. Holland, J. A. Curry, H.-R. Chang, Changes in tropical cyclone number, duration, and intensity in a warming environment. *Science* **309**, 1844–1846 (2005).
8. J. Zhao, R. Zhan, Y. Wang, H. Xu, Contribution of the Interdecadal Pacific Oscillation to the recent abrupt decrease in tropical cyclone genesis frequency over the western North Pacific since 1998. *J. Climate* **31**, 8211–8224 (2018).
9. M. Pazos, B. Mendoza, Landfalling tropical cyclones along the Eastern Pacific coast between the sixteenth and twentieth centuries. *J. Climate* **26**, 4219–4230 (2013).
10. K. J. E. Walsh, J. L. McBride, P. J. Klotzbach, S. Balachandran, S. J. Camargo, G. Holland, T. R. Knutson, J. P. Kossin, T.-c. Lee, A. Sobel, M. Sugi, Tropical cyclones and climate change. *Wiley Interdiscip. Rev. Clim. Change.* **7**, 65–89 (2016).
11. W. Li, L. Li, Y. Deng, Impact of the Interdecadal Pacific Oscillation on tropical cyclone activity in the North Atlantic and Eastern North Pacific. *Sci. Rep.* **5**, 12358 (2015).
12. T. Li, M. Kwon, M. Zhao, J.-S. Kug, J.-J. Luo, W. Yu, Global warming shifts Pacific cyclone locations. *Geophys. Res. Lett.* **37**, L21804 (2010).
13. J. Nakamura, S. J. Camargo, A. H. Sobel, N. Henderson, K. A. Emanuel, A. Kumar, T. E. LaRow, H. Murakami, M. J. Roberts, E. Scoccimarro, P. L. Vidale, H. Wang, M. F. Wehner, M. Zhao, Western North Pacific tropical cyclone model tracks in present and future climates. *J. Geophys. Res. Atmospheres.* **122**, 9721–9744 (2017).
14. H. Murakami, B. Wang, A. Kitoh, Future change of Western North Pacific typhoons: Projections by a 20-km-mesh global atmospheric model. *J. Climate* **24**, 1154–1169 (2011).
15. S. Yokoi, Y. N. Takayabu, H. Murakami, Attribution of projected future changes in tropical cyclone passage frequency over the Western North Pacific. *J. Climate* **26**, 4096–4111 (2013).
16. T. R. Knutson, J. J. Sirutis, M. Zhao, R. E. Tuleya, M. Bender, G. A. Vecchi, G. Villarini, D. Chavas, Global projections of intense tropical cyclone activity for the late twenty-first century from dynamical downscaling of CMIP5/RCP4.5 scenarios. *J. Climate* **28**, 7203–7224 (2015).
17. L. Zhang, K. B. Karnauskas, J. P. Donnelly, K. Emanuel, Response of the North Pacific tropical cyclone climatology to global warming: Application of dynamical downscaling to CMIP5 Models. *J. Climate* **30**, 1233–1243 (2017).
18. C. Zhang, Y. Wang, Projected future changes of tropical cyclone activity over the Western North and South Pacific in a 20-km-mesh regional climate model. *J. Climate* **30**, 5923–5941 (2017).
19. K. Oouchi, J. Yoshimura, H. Yoshimura, R. Mizuta, S. Kusunoki, A. Noda, Tropical cyclone climatology in a global-warming climate as simulated in a 20 km-mesh global atmospheric model: Frequency and wind intensity analyses. *J. Meteorol. Soc. Jpn. Ser II.* **84**, 259–276 (2006).
20. L. Bengtsson, K. I. Hodges, M. Esch, N. Keenlyside, L. Kornblueh, J.-J. Luo, T. Yamagata, How may tropical cyclones change in a warmer climate? *Tellus A Dyn. Meteorol. Oceanogr.* **59**, 539–561 (2007).
21. T. Kohyama, D. L. Hartmann, D. S. Battisti, La Niña–like mean-state response to global warming and potential oceanic roles. *J. Climate* **30**, 4207–4225 (2017).
22. R. Seager, M. Cane, N. Henderson, D.-E. Lee, R. Abernathey, H. Zhang, Strengthening tropical Pacific zonal sea surface temperature gradient consistent with rising greenhouse gases. *Nat. Clim. Chang.* **9**, 517–522 (2019).
23. E.-S. Chung, A. Timmermann, B. J. Soden, K.-J. Ha, L. Shi, V. O. John, Reconciling opposing Walker circulation trends in observations and model projections. *Nat. Clim. Chang.* **9**, 405–412 (2019).
24. S.-P. Xie, Y. Kosaka, What caused the global surface warming hiatus of 1998–2013? *Curr. Clim. Change Rep.* **3**, 128–140 (2017).
25. S.-L. Yao, J.-J. Luo, G. Huang, P. Wang, Distinct global warming rates tied to multiple ocean surface temperature changes. *Nat. Clim. Chang.* **7**, 486–491 (2017).
26. J. C. L. Chan, K. S. Liu, Global Warming and Western North Pacific typhoon activity from an observational perspective. *J. Climate* **17**, 4590–4602 (2004).

27. Z. Wu, N. E. Huang, Ensemble Empirical mode decomposition: A noise-associated data analysis method. *Adv. Adapt. Data Anal.* **01**, 1–41 (2009).
28. C. Qian, C. Fu, Z. Wu, Z. Yan, On the secular change of spring onset at Stockholm. *Geophys. Res. Lett.* **36**, L12706 (2009).
29. C. Qian, On trend estimation and significance testing for non-Gaussian and serially dependent data: Quantifying the urbanization effect on trends in hot extremes in the megacity of Shanghai. *Climate Dynam.* **47**, 329–344 (2016).
30. C. Qian, Z. Wu, C. Fu, D. Wang, On changing El Niño: A view from time-varying annual cycle, interannual variability, and mean state. *J. Climate* **24**, 6486–6500 (2011).
31. T. Lian, Uncertainty in detecting trend: A new criterion and its applications to global SST. *Climate Dynam.* **49**, 2881–2893 (2017).
32. T. Lian, D. Chen, J. Ying, P. Huang, Y. Tang, Tropical Pacific trends under global warming: El Niño-like or La Niña-like? *Natl. Sci. Rev.* **5**, 810–812 (2018).
33. J.-J. Luo, G. Wang, D. Dommenget, May common model biases reduce CMIP5's ability to simulate the recent Pacific La Niña-like cooling? *Climate Dynam.* **50**, 1335–1351 (2018).
34. S. Xie, Ocean warming pattern effect on global and regional climate change. *AGU Adv.* **1**, e2019AV000130 (2020).
35. B. J. Henley, J. Gergis, D. J. Karoly, S. Power, J. Kennedy, C. K. Folland, A tripole index for the Interdecadal Pacific Oscillation. *Climate Dynam.* **45**, 3077–3090 (2015).
36. H.-M. Kim, M.-I. Lee, P. J. Webster, D. Kim, J. H. Yoo, A physical basis for the probabilistic prediction of the accumulated tropical cyclone kinetic energy in the western North Pacific. *J. Climate* **26**, 7981–7991 (2013).
37. R. Zhan, Y. Wang, CFSv2-based statistical prediction for seasonal Accumulated Cyclone Energy (ACE) over the Western North Pacific. *J. Climate* **29**, 525–541 (2016).
38. J. P. Kossin, A global slowdown of tropical-cyclone translation speed. *Nature* **558**, 104–107 (2018).
39. J. T. Prohaska, A technique for analyzing the linear relationships between two meteorological fields. *Mon. Weather Rev.* **104**, 1345–1353 (1976).
40. C. S. Bretherton, C. Smith, J. M. Wallace, An intercomparison of methods for finding coupled patterns in climate data. *J. Climate* **5**, 541–560 (1992).
41. U. Grömping, Relative importance for linear regression in *R*: The package relaimpo. *J. Stat. Softw.* **17**, 1–27 (2006).
42. H. Murakami, B. Wang, T. Li, A. Kitoh, Projected increase in tropical cyclones near Hawaii. *Nat. Clim. Chang.* **3**, 749–754 (2013).
43. S. J. Camargo, M. K. Tippett, A. H. Sobel, G. A. Vecchi, M. Zhao, Testing the performance of tropical cyclone genesis indices in future climates using the HiRAM Model. *J. Climate* **27**, 9171–9196 (2014).
44. L. M. Harris, S.-J. Lin, C. Tu, High-resolution climate simulations using GFDL HiRAM with a stretched global grid. *J. Climate* **29**, 4293–4314 (2016).
45. H. Murakami, G. A. Vecchi, G. Villarini, T. L. Delworth, R. Gudgel, S. Underwood, X. Yang, W. Zhang, S.-J. Lin, Seasonal forecasts of major hurricanes and landfalling tropical cyclones using a high-resolution GFDL coupled climate model. *J. Climate* **29**, 7977–7989 (2016).
46. W. M. Putman, S.-J. Lin, Finite-volume transport on various cubed-sphere grids. *J. Comput. Phys.* **227**, 55–78 (2007).
47. M. Zhao, I. M. Held, S.-J. Lin, G. A. Vecchi, Simulations of global hurricane climatology, interannual variability, and response to global warming using a 50-km resolution GCM. *J. Climate* **22**, 6653–6678 (2009).
48. B. Huang, V. F. Banzon, E. Freeman, J. Lawrimore, W. Liu, T. C. Peterson, T. M. Smith, P. W. Thorne, S. D. Woodruff, H.-M. Zhang, Extended reconstructed sea surface temperature version 4 (ERSST.v4). Part I: Upgrades and intercomparisons. *J. Climate* **28**, 911–930 (2015).
49. G. P. Compo, J. S. Whitaker, P. D. Sardeshmukh, N. Matsui, R. J. Allan, X. Yin, B. E. Gleason, R. S. Vose, G. Rutledge, P. Bessemoulin, S. Brönnimann, M. Brunet, R. I. Crouthamel, A. N. Grant, P. Y. Groisman, P. D. Jones, M. C. Kruk, A. C. Kruger, G. J. Marshall, M. Maugeri, H. Y. Mok, Ø. Nordli, T. F. Ross, R. M. Trigo, X. L. Wang, S. D. Woodruff, S. J. Worley, The twentieth century reanalysis project. *Q. J. Roy. Meteorol. Soc.* **137**, 1–28 (2011).
50. E. Kalnay, M. Kanamitsu, R. Kistler, W. Collins, D. Deaven, L. Gandin, M. Iredell, S. Saha, G. White, J. Woollen, Y. Zhu, M. Chelliah, W. Ebisuzaki, W. Higgins, J. Janowiak, K. C. Mo, C. Ropelewski, J. Wang, A. Leetmaa, R. Reynolds, R. Jenne, D. Joseph, The NCEP/NCAR 40-year reanalysis project. *Bull. Am. Meteorol. Soc.* **77**, 437–472 (1996).

Acknowledgments: We thank L. Tao and L. Chen for providing the computing resources on National Supercomputing Center–Tianhe (NSCC-TJ) server. **Funding:** This work is supported, in part, by the National Natural Science Foundation of China (grants 41875114, 41775060, and 41875057) and, in part, by the Korea Meteorological Administration Research and Development Program under grant KMIPA 2018-03212. **Author contributions:** J.Z. and R.Z. contributed equally in this work, by conceiving parts of this study, conducting the data analyses and model experiments, and drafting the initial manuscript. Y.W. conceived the development of this study. Y.W. and S.-P.X. contributed to the improvement of the manuscript. Q.W. conceived parts of this study. All authors read and approved the manuscript. **Competing interests:** The authors declare that they have no competing interests. **Data and materials availability:** The 1960–2019 June-November (JJASON) best-track TC dataset, including 6-hourly records of TC locations and maximum sustained near-surface wind speed, was obtained from the International Best Track Archive for Climate Stewardship (IBTrACS; www.ncdc.noaa.gov/ibtracs/index.php?name=ibtracs-data). Here, we mainly used the TC genesis and track locations to describe TC activity; the intensity is only used to define TC genesis for a TC reaching 35 knots for the first time in this work. The 1960–2019 Extended Reconstructed SST version 4 (ERSST.V4) (*48*) data were obtained from the NOAA. The 1960 to 2014 NOAA 20C (https://psl.noaa.gov/data/gridded/data.20thC_ReanV2c.html) (*49*) data (version 2) were used to carry out the trend and composite analyses. The National Centers for Environmental Prediction/National Centers for Atmospheric Research reanalysis I (NCEP/NCAR-I; www.esrl.noaa.gov/psd/data/gridded/data.ncep.reanalysis.html) (*50*) data from 1960 to 2019 were used to confirm the results from the NOAA 20C dataset. All data needed to evaluate the conclusions in the paper are present in the paper and/or the Supplementary Materials. Additional model data and codes related to this paper may be requested from the authors.

Submitted 23 December 2019
Accepted 21 August 2020
Published 9 October 2020
10.1126/sciadv.aba6813

Citation: J. Zhao, R. Zhan, Y. Wang, S.-P. Xie, Q. Wu, Untangling impacts of global warming and Interdecadal Pacific Oscillation on long-term variability of North Pacific tropical cyclone track density. *Sci. Adv.* **6**, eaba6813 (2020).